IEEE Access
Multidisciplinary : Rapid Review : Open Access Journal

Received April 18, 2022, accepted April 27, 2022, date of publication May 5, 2022, date of current version May 13, 2022.

Digital Object Identifier 10.1109/ACCESS.2022.3172935

An Ultrawideband Bidirectional Absorptive Common-Mode Filter With All-Pass Signal Transmission

YU-HSIANG CHEN AND CHENG-NAN CHIU, (Senior Member, IEEE)
Department of Electrical Engineering, Yuan Ze University, Taoyuan 32003, Taiwan

Corresponding author: Cheng-Nan Chiu (cnchiu@saturn.yzu.edu.tw)

This work was supported by the Ministry of Science and Technology, Taiwan, under Grant MOST 110-2221-E-155-017.

ABSTRACT This study proposes a miniaturized strip-line absorptive common-mode filter using a novel and ingenious defected ground structure (DGS). The proposed filter is bidirectional and has an ultrawide absorption band to stop the common-mode noise. The fractional bandwidth was as large as 147%. In addition, the filter allows the total transmission of differential signals of up to approximately 15 GHz, as determined by the 3-dB cutoff frequency. Both noise absorption and signal transmission bandwidths have never been reported in the literature. An equivalent circuit model and design principle were proposed. Accordingly, a filter prototype with a total area of 1.1% of the square of the wavelength at the lowest frequency of the absorption band is designed and implemented. The measured results verified the design and demonstrated its claimed performance.

INDEX TERMS Absorptive common-mode filter (A-CMF), common-mode noise, defected ground structure (DGS), differential signal, signal integrity (SI).

I. INTRODUCTION

Differential signaling schemes have been broadly applied in modern digital systems to convey digital signals with high data rate, high speed, low supply voltage, and high noise immunity. Nevertheless, discontinuities and unbalanced signals on differential lines lead to common-mode (CM) noise. This noise may result in the deterioration of signal integrity (SI) or the generation of noticeable electromagnetic interference (EMI) from the lines [1], [2]. Numerous common-mode filters have been developed for the suppression of such noise in the last decade.

These filters can be divided into two types: reflective and absorptive. For the design of reflective common-mode filters, defected ground structures (DGS's) [3]–[7] or mushroom-like electromagnetic bandgap (EBG) structures [8], [9] have been widely adopted. By routing differential lines over the ground embedded with DGS or EBG structures, the currents distributed on the ground can produce equivalent capacitors and inductors to form resonant circuits. While the circuits resonate, common-mode noises are reflected. However, reflected noises from such common-mode filters still exist in the system, which may cause severe SI or EMI problems in the systems. As a result, common mode filters of the absorptive type were invented.

Absorptive common-mode filters (A-CMFs) have been developed in recent years [10]–[24]. The integrated passive device (IPD) process was used in [10] and [11], while the typical printed circuit board (PCB) technology was applied in [11]–[24]. Compared with the IPD process, PCB technology has a lower cost and may achieve better performance. The design of A-CMF can directly add lumped resistors to balanced band-pass filters [14]–[17]. Balanced filter architectures are complex for the total transmission of differential signals. Instead, it can create a broad absorption band by placing differential lines above the DGS, which are added with lumped resistors [19]–[21]. In [21], a DGS with three equal cells having a dumbbell-shaped aperture was proposed to increase the absorption bandwidth by up to 104%. However, the common-mode filter is unidirectional, and the transmission of the differential signal can reach up to 5.5 GHz as shown in Table 1.

In this study, an ultrawideband bidirectional A-CMF is proposed. This filter applies PCB strip-line technology. A new DGS was embedded in the top and bottom ground. Few A-CMF designs have used the strip-line technology. The

The associate editor coordinating the review of this manuscript and approving it for publication was Wen-Sheng Zhao.

TABLE 1. Comparison of the published A-CMF's.

Refs.	Noise absorption band (GHz)	Noise absorption FBW (%)	Signal transmission lower cut-off frequency (GHz)	Signal transmission upper cut-off frequency (GHz)	Process/Layers	Input directions	Size(λ^2)
This work	2.02-13.32	147%	0	14.96	PCB/3	Bidirectional	0.011
[14]	1.51-2.62	58%	1.51	2.62	PCB/2	Bidirectional	0.049
[15]	2.18-4.97	76%	1.38	5.19	PCB/2	Bidirectional	0.051
[16]	1.28-3.76	98%	1.28	3.76	PCB/2	Unidirectional	0.582
[17]	1.2-6.7	139%	0	12	PCB/2	Bidirectional	0.026
[18]	2.2-2.5	12%	0	6.1	PCB/4	Bidirectional	0.005
[19]	1.8-3	50%	0	7.4	PCB/2	Bidirectional	0.140
[20]	1.9-4.1	73%	0	6.4	PCB/4	Unidirectional	0.002
[21]	1.7-5.45	104%	0	5.5	PCB/2	Unidirectional	0.012
[22]	2.33-2.69	14%	0	7.5	PCB/2	Unidirectional	0.036

major advantages of applying this technology are a more compact size and reduced signal distortion owing to the DGS. Therefore, a higher cutoff frequency for the differential signal may be achieved. Here, the differential-signal transmission can reach up to 14.96 GHz. As shown in Table 1, the bandwidths of the signal transmission were the largest in comparison with other published filters.

In addition, the newly proposed filter employs an innovative and easily designed DGS with five cells and three types of dumbbell-shaped apertures. This DGS increases the absorption bandwidth by 147%. In addition, the absorption bandwidth was the largest among the published filters, as shown in Table 1.

A DGS can be easily designed because its physical mechanism is clear. The design principle and equivalent circuit model were presented. Accordingly, a filter prototype was designed, fabricated, and tested. There was good agreement between the measurement and simulation. The measured results verify the filter performance stated above.

II. BIDIRECTIONAL STRIP-LINE A-CMF DESIGN

A. FILTER CONFIGURATION AND ITS BENCHMARK PERFORMANCE

The configuration of the proposed strip-line A-CMF is illustrated in Fig. 1. As shown in Fig. 1(a), the differential lines were sandwiched between the top and bottom ground planes. The differential lines shown in Fig. 1(b) can be divided into three sections: the left, center, and right. In the center section, the distance between the two strips was intentionally reduced to induce strong coupling. This improves differential signal transmission. Nevertheless, a differential-mode (DM) characteristic impedance of 100 Ω was maintained along the entire length, including the three sections.

A DGS with five cells was embedded in the top and bottom planes. These five cells can be classified into three types, as shown in Fig. 1(c). The arrangement of the five cells on each ground plane was symmetric to realize the bidirectional characteristics of the filter. For impedance matching and absorption of CM noise, four lumped resistors with two different values, R1 and R2, were added to the four smaller cells. Similarly, the arrangement should consider bidirectional symmetry.

A filter prototype was designed and implemented using a printed PCB strip-line structure with two dielectric layers and three metal layers. Each dielectric layer was a RO4003C substrate with a thickness of 0.406 mm, dielectric constant of 3.55, and loss tangent of 0.0027. The DGS is added to the top and bottom metal layers or ground planes. The geometric parameters of the DGS are: p1 = 2 mm, p2 = 4 mm, p3 = 7 mm, b1= 0.5 mm, b2 = 0.55 mm w1 = 5.5 mm, w2 = 7.5mm, P = 12.5 mm, W = 21.1 mm, w3 = w5 = 3.5 mm, w4 = 2.5mm, m1 = 3.8 mm, m2 = 3 mm, m3 = 0.2 mm and u1 = u2 = 0.8 mm. Two metal strips are placed on the central metal layer. Their related dimensions are: wp = 0.35 mm, ws = 0.3 mm, d1 = 0.8 mm, d2 = 0.3 mm.

The benchmark performance of the designed filter is shown in Fig. 2. The results were simulated using a full-wave simulator, HFSS [25]. The differential-signal reflection and transmission, CM noise reflection and transmission, and differential-signal group delays are shown in Fig. 2(a), 2(b), and 2(c), respectively. The differential-signal transmission can be up to approximately 15 GHz, which is determined by the 3-dB insertion loss. In addition, the CM noise absorption band should be determined by the 10-dB return loss and the 10-dB insertion loss. As shown in Fig. 2(b), the overlapped band is from 2.02 GHz to 13.32 GHz, which is equal to a fractional bandwidth (FBW) of 147%. Compared to the published A-CMFs in Table 1, the proposed filter outperforms all others. The differential signal group delays fed from both directions are shown in Fig. 2(c). Again, the flatness and equality of the delays demonstrate the bidirectional characteristics and ultrawideband signal transmission.

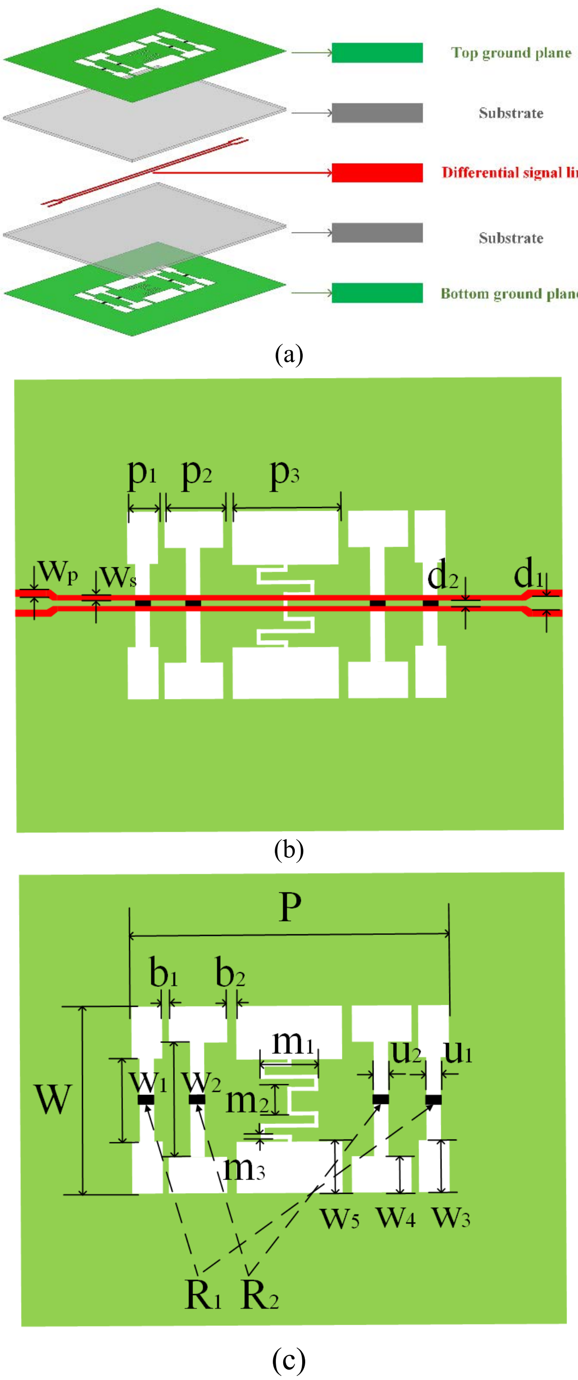

FIGURE 1. Configuration of the proposed A-CMF. (a) Layer stack-up. (b) Differential signal lines. (c) Top and bottom ground planes.

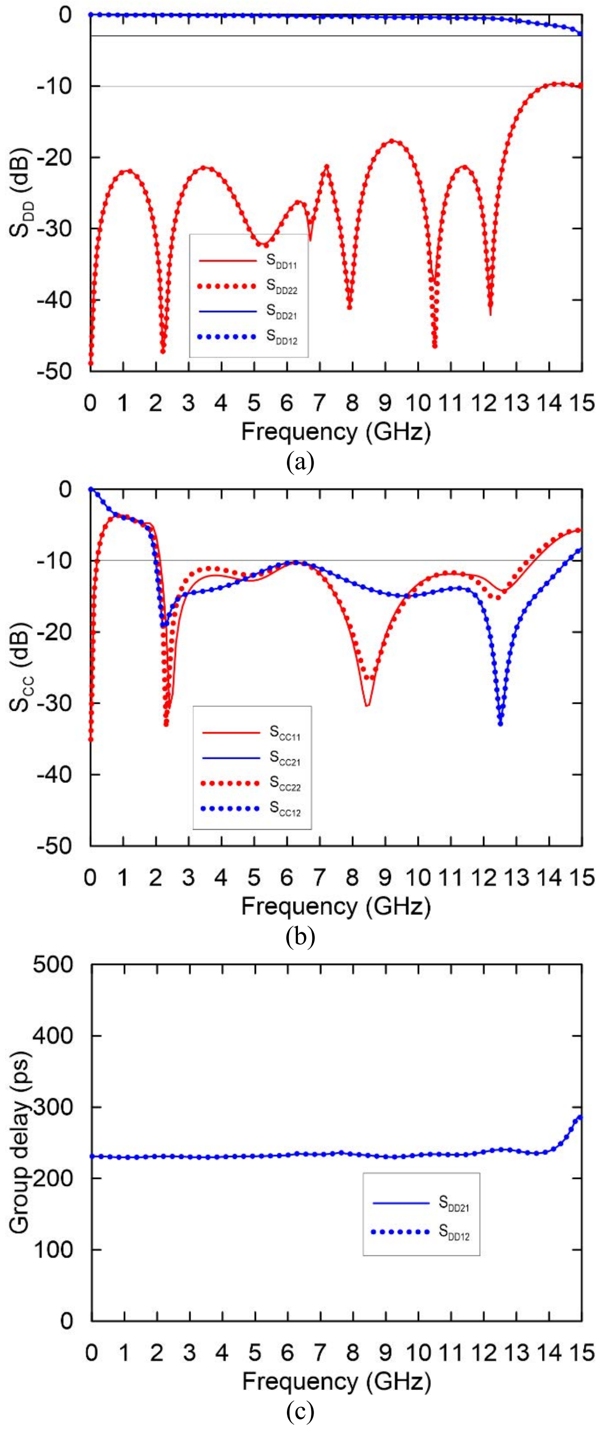

FIGURE 2. Benchmark performance of the proposed A-CMF. (a) Reflection and transmission of differential signal. (b) Reflection and transmission of CM noise. (c) Group delay of differential signal.

B. PHYSICAL MECHANISM AND DESIGN PRINCIPLE

The physical mechanism of the proposed A-CMF was clear. Three types of DGS cells (as shown in Fig. 3(a), 3(c), and 3(e)) can generate three different resonances. Their equivalent circuits are shown in Fig. 3(b), 3(d), and 3(f). It is essential that the largest center cell (Fig. 3(e)) should be a dual-band resonant circuit. The entire aperture generates lower-frequency resonance, whereas the central ribbon-like slot creates higher-frequency resonance.

The CM current distributions of the three cells corresponding to the first, second, and third dips in Figure 2(b) are shown in Fig. 4. By observing these current distributions, it is clear that the largest cell is responsible for both the lowest and highest resonant frequencies. The two smaller cells had resonant frequencies between the lowest and highest resonant frequencies.

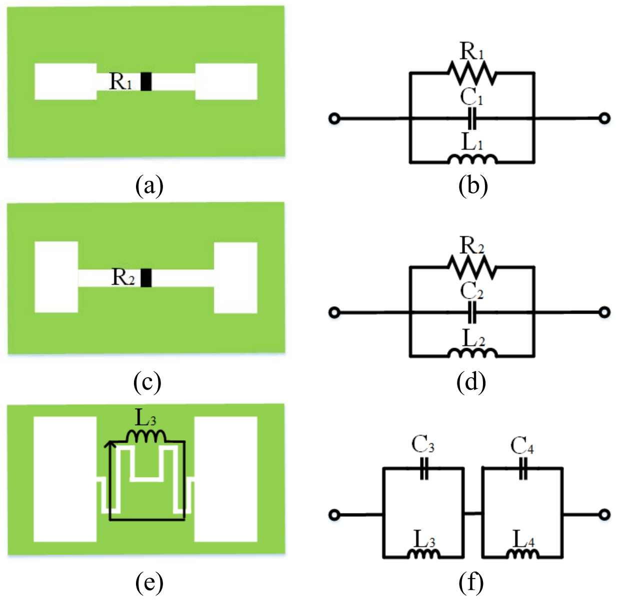

FIGURE 3. Physical mechanism of each DGS cell. (a) The smallest DGS cell. (b) Equivalent circuit of the smallest cell. (c) The middle DGS cell. (d) Equivalent circuit of the middle cell. (e) The largest DGS cell. (f) Equivalent circuit of the largest cell.

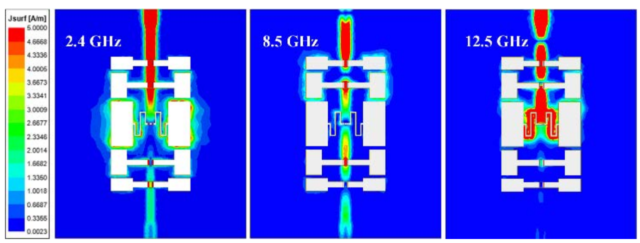

FIGURE 4. The current distributions on the DGS at lowest, middle and highest resonant frequencies.

TABLE 2. Component values of the equivalent circuit.

Parameters	Value (nH)	Parameters	Value (pF)
L_1	1.77	C_1	0.33
L_2	2.21	C_2	0.23
L_3	0.18	C_3	0.91
L_4	3.65	C_4	1.51

The evolution of A-CMF may follow the steps shown in Fig. 5(a). This changed from Type A to Type D. As shown in Fig. 5(b), the filter evolved from a dual-stop-band filter to an ultrawide band-stop filter. It is important to mention again that the two resonant frequencies of Type A (or the largest center cell) determine the upper and lower limits of the absorption band. Consequently, it is convenient to quickly predict the absorption band based on the largest cell.

C. EQUIVALENT CIRCUIT

Based on the above discussion, the CM equivalent circuit model of the proposed filter is shown in Fig. 6. There are five resonant circuits of three different types: two single-band and one dual-band. In particular, the center resonant circuit has two resonant frequencies that determine the upper and lower limits of the absorption band. The component values can be extracted using Q3D [26], and are summarized in Table 2.

Figure 7 shows the results obtained by the equivalent circuit and full-wave simulation. The results agree well with each other. Therefore, the equivalent circuit model can be applied for the initial guess of the design.

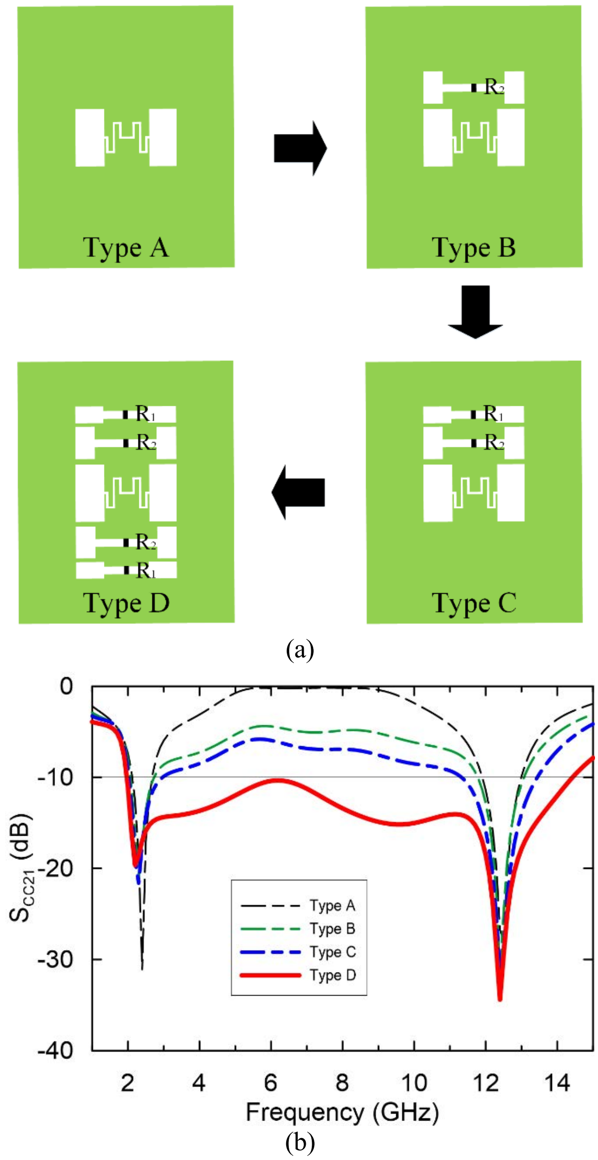

FIGURE 5. Evolution of the A-CMF. (a) The evolution steps. (b) The corresponding responses.

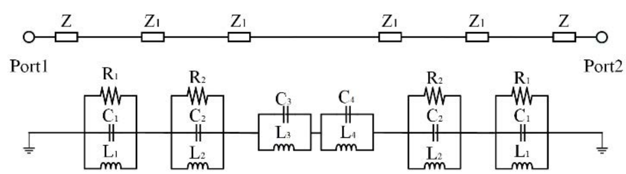

FIGURE 6. CM equivalent circuit of the proposed A-CMF.

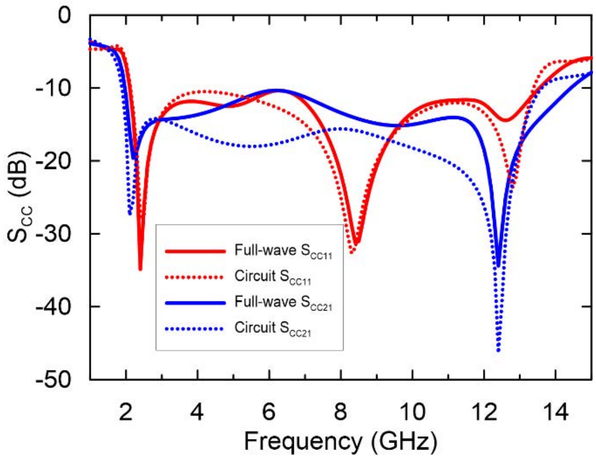

FIGURE 7. Comparison between circuit and full-wave simulations.

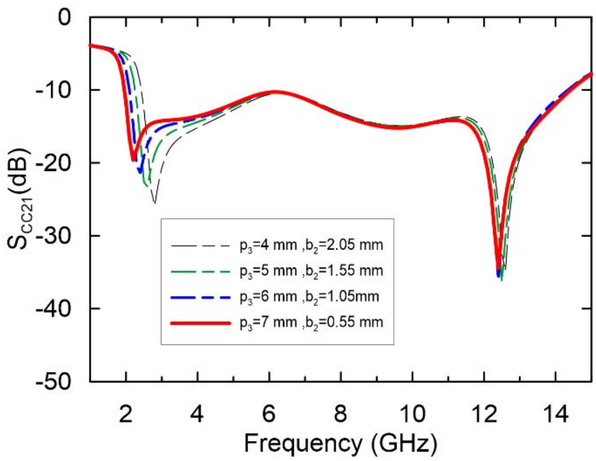

(a)

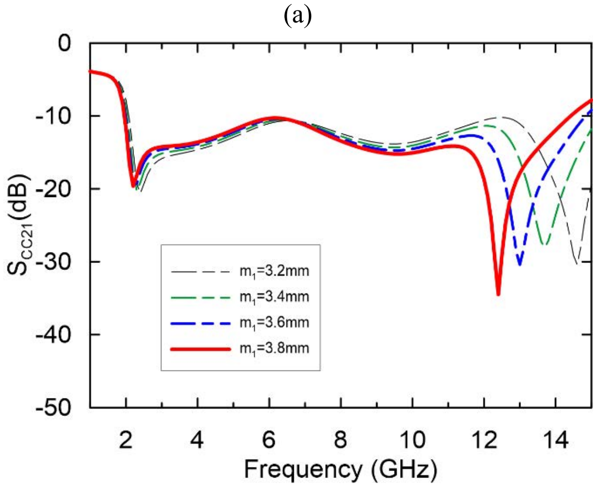

(b)

FIGURE 8. Performance variations due to the geometrical parameters of the largest DGS cell.

D. GEOMETRY AND RESISTOR PARAMETER ANALYSIS

As the evolution of the filter is revealed, its bandwidth highly depends on the largest center cell of the DGS. As shown in Fig. 3, this cell is equivalent to a dual-band resonant circuit. The lower and upper resonant frequencies determine the band limit. Fig. 8 shows a study of the geometric parameters of this cell, as indicated in Fig. 1. The key parameters in

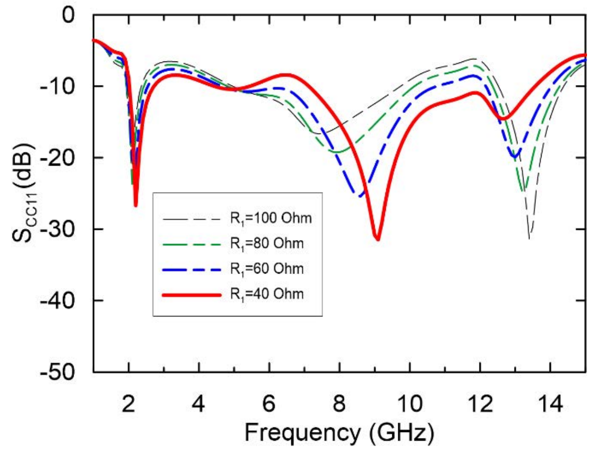

(a)

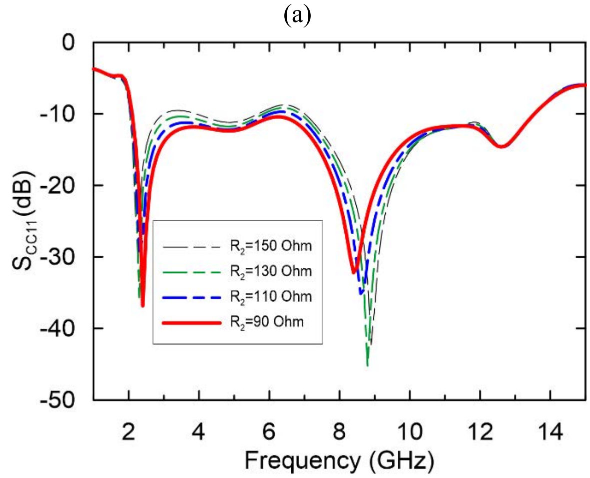

(b)

FIGURE 9. Performance variations due to the resistances of: (a) R1, (b) R2.

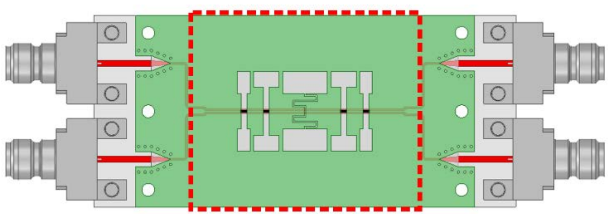

(a)

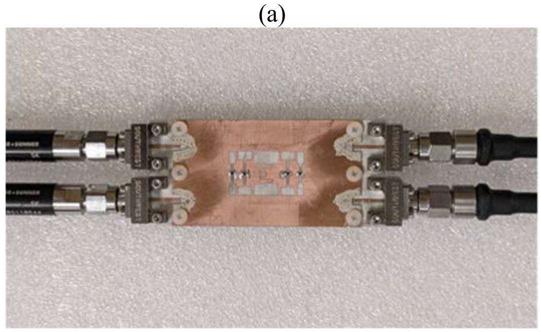

(b)

FIGURE 10. The implemented prototype: (a) its configuration, (b) its photo.

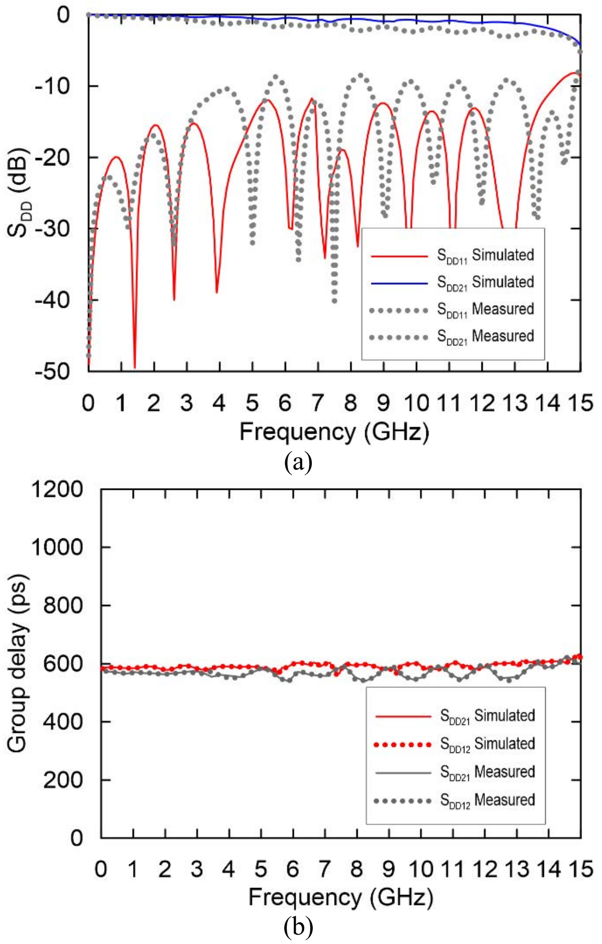

FIGURE 11. Comparison of differential signals. (a) Reflection and transmission. (b) Group delay.

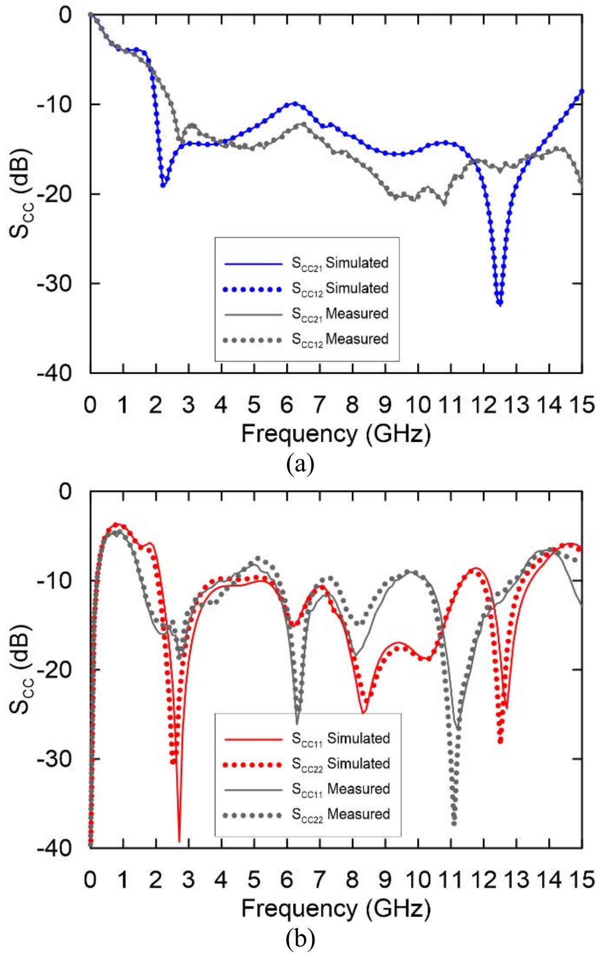

FIGURE 12. Comparison of CM noise in the frequency domain. (a) Transmission. (b) Reflection.

Fig. 8(a) and (b) are related to variations in the lower and upper band limits, respectively.

The added resistors are primarily used for impedance matching of the CM noise. After the noise enters the filter, the resistors dissipate energy. As shown in Fig. 9, the value of R1 has a major effect on the matching performance, while the value of R2 is applied for fine-tuning. When R1 and R2 are set to 40 and 90 Ω, respectively, the bandwidth can be maximized. Here, the absorption band was from 2.02 GHz to 13.32 GHz. By comparing Fig. 8 and 9, the stop-band determined by the 10-dB insertion loss could be wider which is from 1.98 GHz to 14.53 GHz. This is because the CM noise can be stopped by the absorption or reflection mechanism. However, the reflected noise may not be favorable for some applications.

III. IMPLEMENTATION AND EXPERIMENT

A. FILTER IMPLEMENTATION

A prototype of the A-CMF was fabricated, as shown in Fig. 10. To connect the SMA connectors for measurement, a transition method [27] from a strip line to a microstrip line was applied. Subsequently, four high-frequency SMA connectors were connected to the ports. For a better comparison, the connector effect was considered and modelled in the simulation.

B. EXPERIMENTAL VALIDATION

The frequency- and time-domain experimental validations are shown in Fig. 11, 12, and 13, respectively. Fig. 11 displays the simulated and measured S-parameters and group delays of the differential signal. Fig. 12 shows the simulated and measured S-parameters of the CM noise. These figures show the agreement between the simulation and the measurement. In addition, the bidirectional performance was confirmed again. However, the measurement was not exactly the same as the simulation. This is because of the non-ideal effects of the materials, fabrication uncertainties, and measurement setup. Because the frequency band of concern is extremely wide, the substrate dielectric constant and loss tangent are dispersive and could not be modeled accurately in the simulation. In addition, many structural lines and slots are very narrow and would have dimensional uncertainties during fabrication. The measurement setup required SMA connectors soldered with transitions from a strip line to a microstrip line. The setup also causes unavoidable differences between the measurements and simulations.

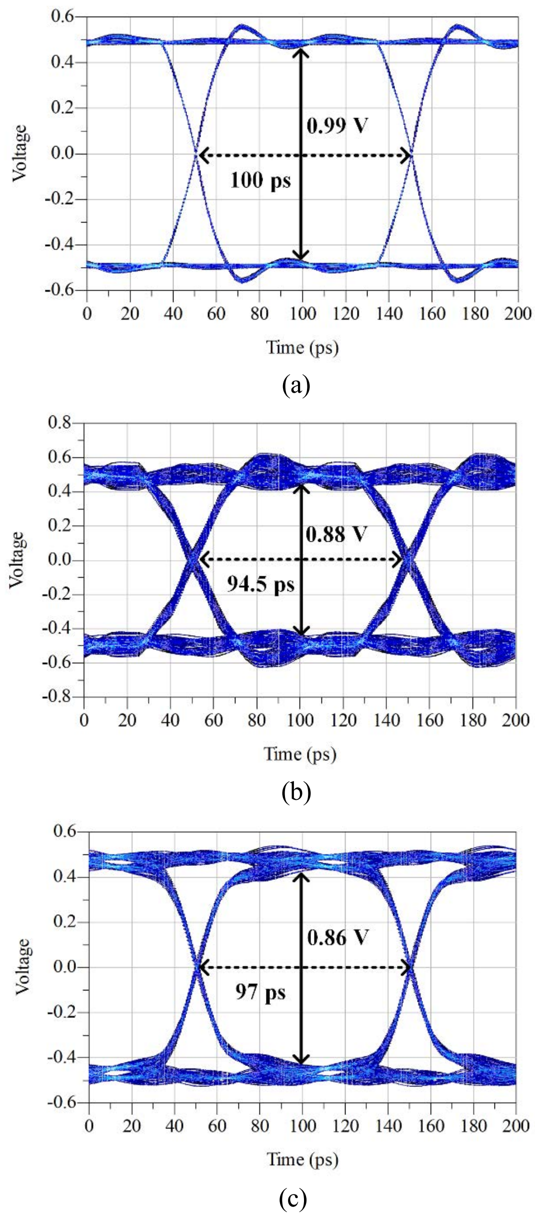

FIGURE 13. Comparison of the time-domain results. Eye diagrams of: (a) the reference board, (b) the A-CMF by simulation, (c) the A-CMF by measurement.

Figure 13 shows simulated and measured eye diagrams. The digital signal had a data rate of 10 Gb/s and a rise/fall time of 20 ps. An eye diagram of the reference board is shown in Fig. 13(a). Its eye height and width are 0.99 V and 100 ps, respectively. As with the A-CMF, the simulated eye height and width were reduced to 0.88 V and 94.5 ps. The measured eye height and width are, respectively, reduced to 0.86 V and 97 ps. The performance is remarkable for the SI requirements.

IV. CONCLUSION

A compact bidirectional A-CMF using PCB strip-line technology and employing an innovative DGS is proposed and studied herein. Its noise absorption band is ultrawide and can reach up to 147% FBW. Its signal transmission band ranges from DC to 15 GHz. Based on the noise absorption and signal transmission bandwidths, the proposed design is the best among all published filters. However, minimizing the sample size could be a future study. An equivalent circuit model and design principle were proposed for the filter design. Accordingly, a filter prototype was implemented and measured. Both the frequency- and time-domain results validate the design and demonstrate the practicality of the filter for modern high-speed digital applications.

REFERENCES

[1] T.-L. Wu, F. Buesink, and F. Canavero, "Overview of signal integrity and EMC design technologies on PCB: Fundamentals and latest progress," *IEEE Trans. Electromagn. Compat.*, vol. 55, no. 4, pp. 624–638, Aug. 2013.

[2] D. M. Hockanson, J. L. Drewniak, T. H. Hubing, T. P. Van Doren, F. Sha, and M. J. Wilhelm, "Investigation of fundamental EMI source mechanisms driving common-mode radiation from printed circuit boards with attached cables," *IEEE Trans. Electromagn. Compat.*, vol. 38, no. 4, pp. 557–566, Nov. 1996.

[3] W.-T. Liu, C.-H. Tsai, T.-W. Han, and T.-L. Wu, "An embedded common-mode suppression filter for GHz differential signals using periodic defected ground plane," *IEEE Microw. Wireless Compon. Lett.*, vol. 18, no. 4, pp. 248–250, Apr. 2008.

[4] S.-J. Wu, H.-H. Chuang, T.-K. Wang, and T.-L. Wu, "A novel HU-shaped common-mode filter for GHz differential signals," in *Proc. IEEE Int. Symp. Electromagn. Compat.*, Aug. 2008, pp. 1–4.

[5] S.-J. Wu, C.-H. Tsai, T.-L. Wu, and T. Itoh, "A novel wideband common-mode suppression filter for gigahertz differential signals using coupled patterned ground structure," *IEEE Trans. Microw. Theory Techn.*, vol. 57, no. 4, pp. 848–855, Apr. 2009.

[6] Z. Zeng, Y. Yao, and Y. Zhuang, "A wideband common-mode suppression filter with compact-defected ground structure pattern," *IEEE Trans. Electromagn. Compat.*, vol. 57, no. 5, pp. 1277–1280, Oct. 2015.

[7] L.-H. Zhou, Y.-L. Ma, J. Shi, J.-X. Chen, and W. Che, "Differential dual-band bandpass filter with tunable lower band using embedded DGS unit for common-mode suppression," *IEEE Trans. Microw. Theory Techn.*, vol. 64, no. 12, pp. 4183–4191, Dec. 2016.

[8] Q. Liu, S. Connor, C. Olivieri, F. De Paulis, A. Orlandi, M. A. Cracraft, B. Archambeault, and V. V. Khilkevich, "Reduction of EMI due to common-mode currents using a surface-mount EBG-based filter," *IEEE Trans. Electromagn. Compat.*, vol. 58, no. 5, pp. 1440–1447, Oct. 2016.

[9] C.-Y. Hsiao, C.-H. Tsai, C.-N. Chiu, and T.-L. Wu, "Radiation suppression for cable-attached packages utilizing a compact embedded common-mode filter," *IEEE Trans. Compon., Packag., Manuf. Technol.*, vol. 2, no. 10, pp. 1696–1703, Oct. 2012.

[10] C.-Y. Hsiao, C.-H. Cheng, and T.-L. Wu, "A new broadband common-mode noise absorption circuit for high-speed differential digital systems," *IEEE Trans. Microw. Theory Techn.*, vol. 63, no. 6, pp. 1894–1901, Jun. 2015.

[11] C.-K. Chan and T.-L. Wu, "A high-performance common-mode noise absorption circuit based on phase modification technique," *IEEE Trans. Microw. Theory Techn.*, vol. 67, no. 11, pp. 4394–4403, Nov. 2019.

[12] L.-H. Zhou, Y.-L. Ma, J. Shi, J.-X. Chen, and W. Che, "Differential dual-band bandpass filter with tunable lower band using embedded DGS unit for common-mode suppression," *IEEE Trans. Microw. Theory Techn.*, vol. 63, no. 12, pp. 1894–1901, Dec. 2015.

[13] P.-J. Li, Y.-C. Tseng, C.-H. Cheng, and T.-L. Wu, "A novel absorptive common-mode filter for cable radiation reduction," *IEEE Trans. Compon., Packag., Manuf. Technol.*, vol. 7, no. 4, pp. 511–518, Apr. 2017.

[14] W. Zhang, Y. Wu, Y. Liu, C. Yu, A. Hasan, and F. M. Ghannouchi, "Planar wideband differential-mode bandpass filter with common-mode noise absorption," *IEEE Microw. Wireless Compon. Lett.*, vol. 27, no. 5, pp. 458–460, May 2017.

[15] Y. Guan, Y. Wu, and M. M. Tentzeris, "A bidirectional absorptive common-mode filter based on interdigitated microstrip coupled lines for 5G 'Green' communications," *IEEE Access*, vol. 8, pp. 20759–20769, 2020.

[16] Y. Zhu, K. Song, M. Fan, S. Guo, Y. Zhou, and Y. Fan, ''Wideband balanced bandpass filter with common-mode noise absorption using double-sided parallel-strip line,'' *IEEE Microw. Wireless Compon. Lett.*, vol. 30, no. 4, pp. 359–362, Apr. 2020.
[17] Y. Zhu, K. Song, M. Fan, S. Guo, Y. Zhou, and Y. Fan, ''Common-mode noise absorption circuit using double-sided parallel-strip line,'' *IEEE Microw. Wireless Compon. Lett.*, vol. 31, no. 1, pp. 25–28, Jan. 2021.
[18] P.-J. Li and T.-L. Wu, ''A novel circuit architecture of bidirectional common-mode noise absorption circuit,'' *IEEE Trans. Microw. Theory Techn.*, vol. 68, no. 4, pp. 1476–1486, Apr. 2020.
[19] C.-H. Cheng and T.-L. Wu, ''Analysis and design method of a novel absorptive common-mode filter,'' *IEEE Trans. Microw. Theory Techn.*, vol. 67, no. 5, pp. 1826–1834, May 2019.
[20] P.-J. Li and T.-L. Wu, ''Synthesized method of dual-band common-mode noise absorption circuits,'' *IEEE Trans. Microw. Theory Techn.*, vol. 67, no. 4, pp. 1392–1400, Apr. 2019.
[21] S.-K. Tseng, C.-N. Chiu, Y.-C. Tsao, and Y.-P. Chiou, ''A novel ultrawideband absorptive common-mode filter design using a miniaturized and resistive defected ground structure,'' *IEEE Trans. Electromagn. Compat.*, vol. 63, no. 1, pp. 66–73, Feb. 2021.
[22] H.-W. Liu, C.-H. Cheng, P.-J. Li, and T.-L. Wu, ''A novel compact single-stage absorption common-mode filter,'' *IEEE Trans. Electromagn. Compat.*, vol. 64, no. 1, pp. 111–118, Feb. 2022.
[23] T. Adiprabowo, D.-B. Lin, Y.-H. Zheng, Y.-H. Chen, C.-Y. Zhuang, and B.-H. Tsai, ''Dual-band high absorbing and broadband suppressing common-mode noise filter,'' *IEEE Trans. Electromagn. Compat.*, vol. 64, no. 2, pp. 386–395, Apr. 2022.
[24] W. T. Li, H. R. Zhang, X. J. Chai, Y. Q. Hei, J. C. Mou, and X. W. Shi, ''Compact dual-band Balanced-to-Unbalanced filtering power divider design with extended common-mode suppression bandwidth,'' *IEEE Microw. Wireless Compon. Lett.*, early access, Feb. 3, 2022, doi: 10.1109/LMWC.2022.3145021.
[25] (2021). *ANSYS HFSS Website*. [Online]. Available: http://www.ansys.com/products/electronics/ansys-hfss
[26] (2021). *ANSYS Q3D Website*. [Online]. Available: http://www.ansys.com/products/electronics/ansys-q3d-extractor
[27] T. Maleszka and G. Jaworski, ''Broadband stripline to microstrip transition with constant impedance field matching section for applications in multilayer planar technologies,'' in *Proc. 18th Int. Conf. Microw., Radar, Wireless Commun.*, Vilnius, Lithuania, Jun. 2010, pp. 1–4.

YU-HSIANG CHEN was born in Taoyuan, Taiwan, in 1997. He received the B.S. degree in electrical engineering from Yuan Ze University, Taoyuan, in 2020, where he is currently pursuing the M.S. degree in electrical engineering. His main research interest includes common-mode filters for modern digital systems.

CHENG-NAN CHIU (Senior Member, IEEE) received the B.S. degree in physics from the National Tsinghua University, Hsinchu, Taiwan, in 1990, and the M.S. and Ph.D. degrees in electrical engineering from the National Taiwan University, Taipei, Taiwan, in 1993 and 1996, respectively.

From 1996 to 1998, he was with Acer Inc. and Tatung Inc., Taipei. In 1998, he joined the Computer and Communications Laboratory, Industrial Technology Research Institute, Hsinchu. From 2000 to 2015, he was with the Department of Electrical Engineering, Da-Yeh University, Changhua. He was the Chairman of the International Program in Electrical and Communication Engineering with Yuan Ze University, Taoyuan, from 2016 to 2019, where he has been a Professor with the Department of Electrical Engineering, since 2016. His research interests include the electromagnetic compatibility of electronic systems and ICs, the antennas for modern communication systems, and the electromagnetic issues and applications of metamaterials. He has been the Secretary of the IEEE EMC-S Taipei Chapter, since 2014, where he is currently the Chapter Chair. Since 2020, he has been the Associate Editor of the IEEE TRANSACTIONS ON ELECTROMAGNETIC COMPATIBILITY and he is also the Guest Editor of the 2022 Special Issue on Advances and Perspectives in Electromagnetic Shielding and Absorbers.